Electronic Supplementary Information

Enhanced Interface Stability of Ammine Magnesium Borohydride by *in situ* Decoration of MgBr$_2$·2NH$_3$ Nanoparticles

Qian Wang[a,b], Zhaoyue Li[b], Hanyu Deng[c], Yungui Chen[a,d], Yigang Yan[a,d]*

[a] Institute of New Energy and Low-Carbon Technology, Sichuan University, Chengdu 610065, China

[b] College of Materials Science and Engineering, Sichuan University, Chengdu 610065, China

[c] College of Biomass Science and Engineering, Sichuan University, Chengdu 610065, China

[d] Engineering Research Center of Alternative Energy Materials and Devices, Ministry of Education, China

Corresponding author. E-mail: yigang.yan@scu.edu.cn

Experimental Section

Material preparation. 3 g mixture of $NaBH_4$ and $MgBr_2$ was mechanically milled in a 50 mL sealed WC kentanium milling jar at 400 rpm for 2 h with a ball-to-sample mass ratio of 30:1 using a planetary ball mill (PMQ0.4L). The spherical grinding product was transferred to a reaction flask with a filtration device under argon atmosphere and was stirred in anhydrous ether for 0.5h. Afterward, the obtained solution with $Mg(BH_4)_2$ and $MgBr_2$ dissolved was transferred to another flask and was fed with dry ammonia gas to synthesize $Mg(BH_4)_2 \cdot 6NH_3$-$MgBr_2 \cdot 6NH_3$ mixture. $Mg(BH_4)_2$ was synthesized according to the protocol described in the literature.[1] $Mg(BH_4)_2 \cdot 6NH_3$ was prepared from $Mg(BH_4)_2$ and dry ammonia gas. The $Mg(BH_4)_2$ powder was exposed to 1 bar NH_3 atmosphere for 2 h at room temperature. $Mg(BH_4)_2 \cdot 1.9NH_3$-$MgBr_2 \cdot 2NH_3$ composites and $Mg(BH_4)_2 \cdot 1.9NH_3$ were obtained by heating $Mg(BH_4)_2 \cdot 6NH_3$-$MgBr_2 \cdot 6NH_3$ composites and $Mg(BH_4)_2 \cdot 6NH_3$ at 110°C for 4 h under dynamic vacuum, respectively. All sample handlings were performed under Ar atmosphere.

Structural characterization. The measurements of X-ray diffraction (XRD) were conducted at room temperature using a diffractometer (DX-2700B) equipped with a rotating Cu anode (Cu Kα radiation, 2 kW, λ = 1.54056 Å). The samples were packed in 0.5 mm borosilicate capillaries and sealed in an argon atmosphere. Fourier-transform infrared (FTIR) spectra were obtained using a Thermo Fisher Nicolet iS50 ATR spectrometer with a resolution of 4 cm^{-1}. The observation of High-resolution transmission electron microscopy (HRTEM) was carried out using JEOL JEM-F200 coupled with energy-dispersive X-ray spectroscopy (EDS). Inductively coupled plasma Optical Emission Spectrometer (ICP-OES, Agilent 5110, Agilent Technologies, USA) was used to

analyze the concentration of elemental Br in the degradation products. The X-ray photograph spectroscopy (XPS) spectra were recorded on Thermo Scientific K-Alpha+, XPS system. The spectra were corrected based on C 1s binding energy at 284.8 eV. Thermogravimetric Analysis (TGA) measurements were conducted on a Netzsch STA 2500 instrument with a ramp of 10 °C min^{-1} under Ar atmosphere.

Electrochemical Measurements. Measurements of electrochemical impedance spectroscopy (EIS), DC polarization and cyclic voltammetry (CV) tests were performed using Multi Autolab M204 electrochemical workstation. All pellets were prepared in an Ar-filled glovebox with a diameter of 6 mm and a thickness of ~1 mm under a pressure of 0.3 GPa and assembled in a Swagelok-type cell. An asymmetric Mg| SSEs |SS cell configuration and used for cyclic voltammetry (scan rate 10 mV/s). EIS data were measured using a sine perturbation signal of 5mV with the frequency from 1 MHz to 0.1 Hz. High purity Au films were used as blocking electrodes. Galvanostatic cycling was conducted with LANDCT2001A battery tester at 323 K. For the galvanostatic cycling in the symmetric Mg| Mg(BH$_4$)$_2$·1.9NH$_3$-MgBr$_2$·2NH$_3$ |Mg cell.
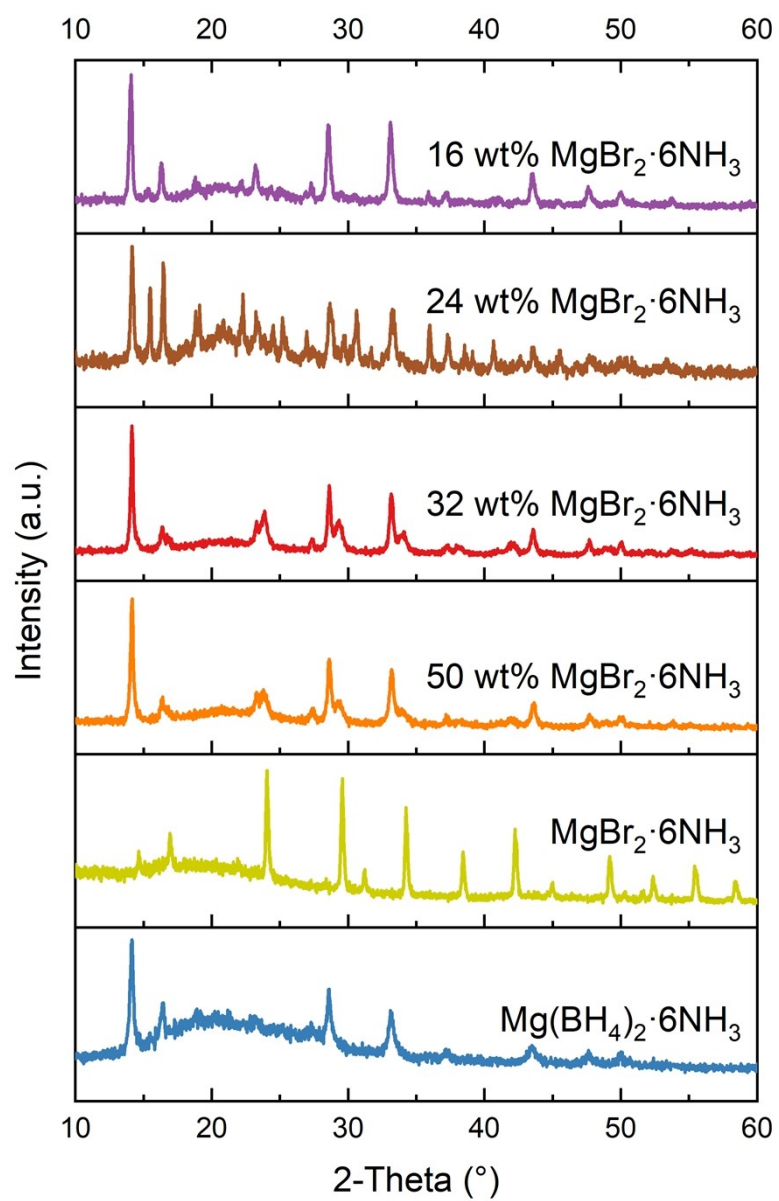
Figure S1. XRD patterns of $Mg(BH_4)_2 \cdot 6NH_3$-$MgBr_2 \cdot 6NH_3$ composites.
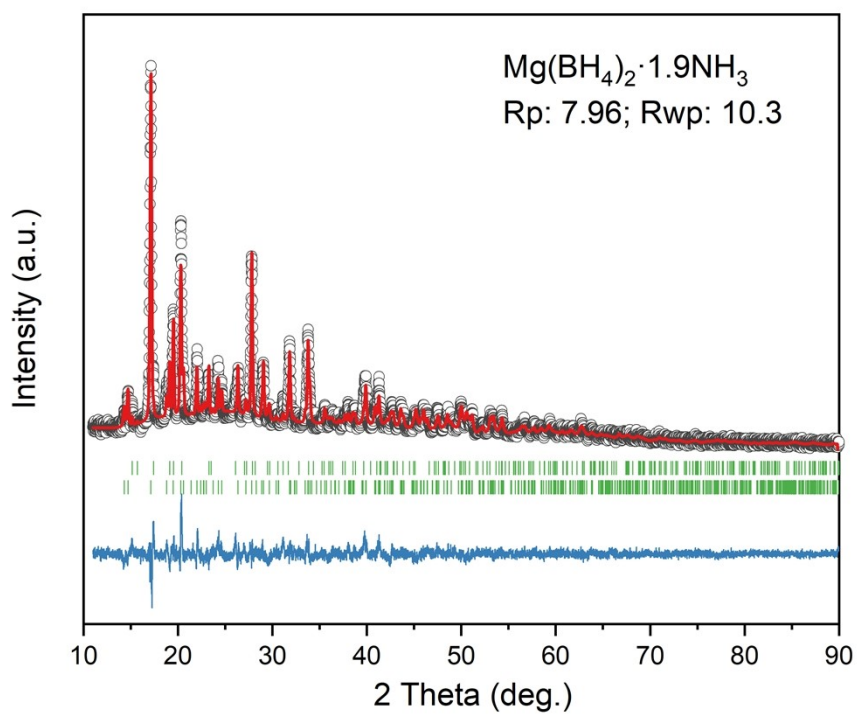
Figure S2. Rietveld refinement of XRD data for $Mg(BH_4)_2 \cdot 1.9NH_3$, showing observed (black circles) and calculated (red line) curves, and a different curve below (blue line). Reflections corresponding to $Mg(BH_4)_2 \cdot NH_3$ (top trick), $Mg(BH_4)_2 \cdot 2NH_3$ (bottom trick). Final discrepancy factors, R_p and R_{wp} (not corrected for background) are shown.
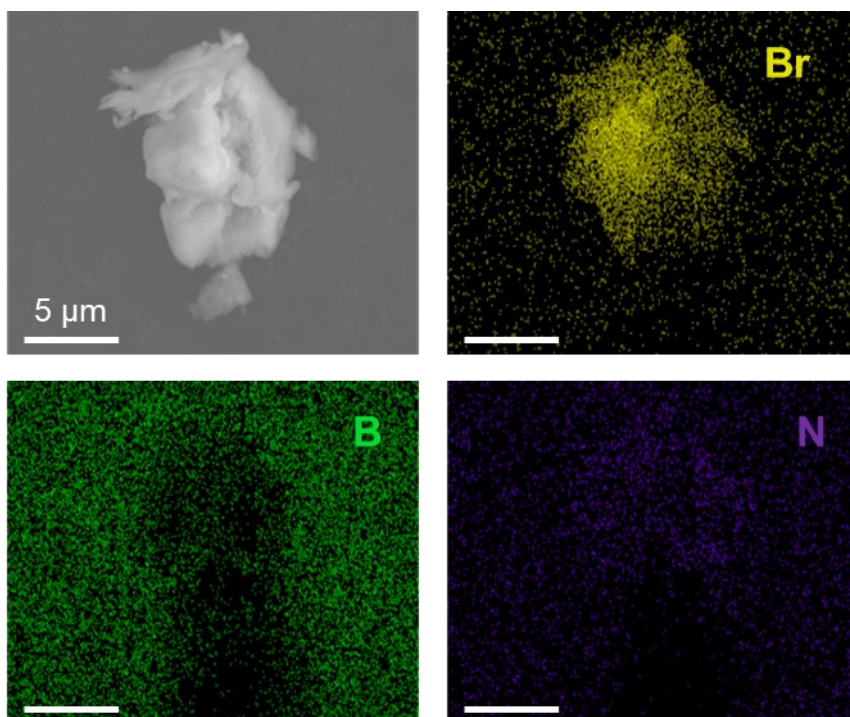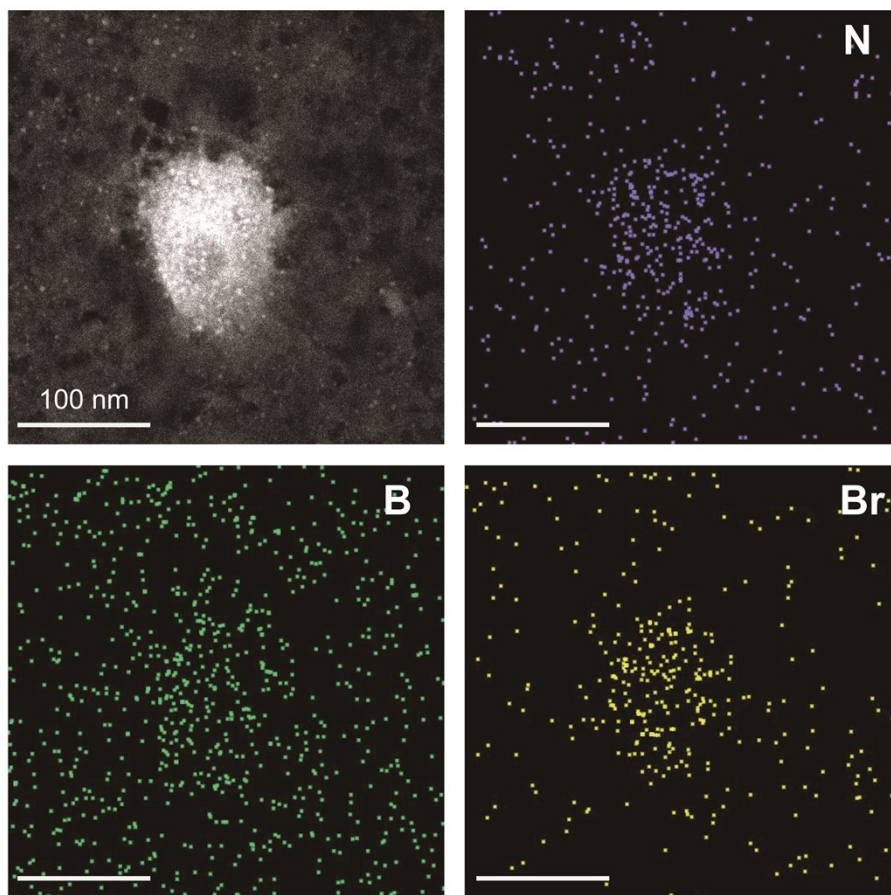
Figure S3. SEM and SEM-EDS images Mg(BH$_4$)$_2$·1.9NH$_3$-32 wt.% MgBr$_2$·2NH$_3$ composite.

Table S1. The crystal plane parameters of $MgBr_2 \cdot 2NH_3$

2θ (°)	(hkl)	d_{cal} (nm)	d_{obs} (nm)
30.913	(121)	0.289	0.300
37.736	(201)	0.238	0.250

The d_{cal} and d_{obs} are lattice fringe spacing from the standard $MgBr_2 \cdot 2NH_3$ (JCPDS 89-6789) and $MgBr_2 \cdot 2NH_3$ in the $Mg(BH_4)_2 \cdot 1.9NH_3$-32 wt.% $MgBr_2 \cdot 2NH_3$ composite observed by HRTEM (Fig. 1c).

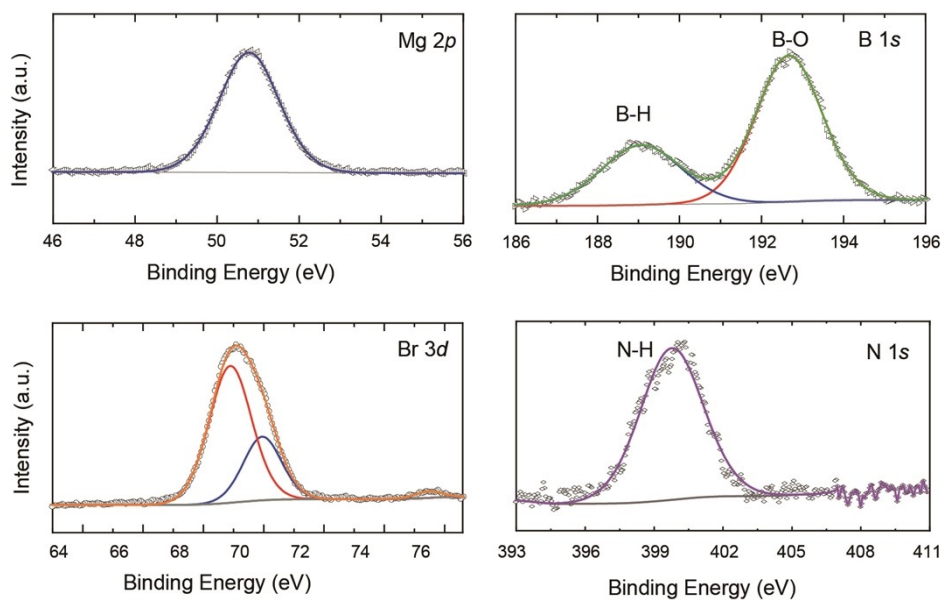**Figure S4.** The STEM-EDS mapping images of Mg(BH$_4$)$_2$·1.9NH$_3$-32 wt.% MgBr$_2$·2NH$_3$ composite. The presence of Mg(BH$_4$)$_2$·1.9NH$_3$ can be verified by the B spectrum.
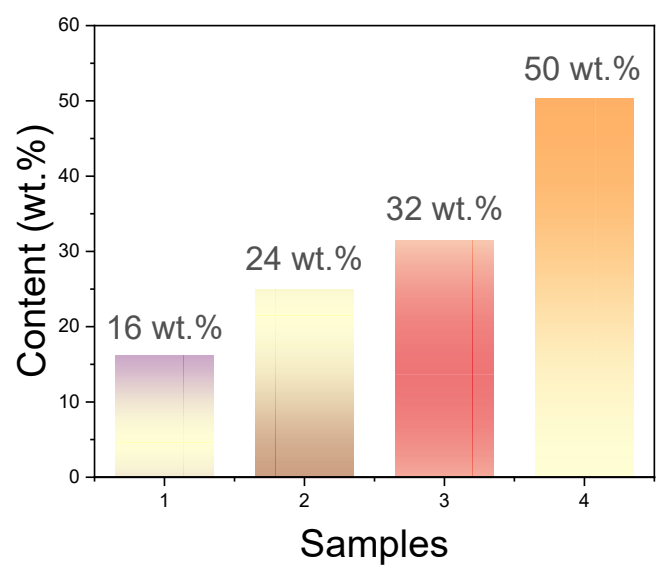
Figure S5. ICP-OES spectra of the $Mg(BH_4)_2 \cdot 1.9NH_3$-x wt.% $MgBr_2 \cdot 2NH_3$ composites (x=16, 24, 32 and 50).
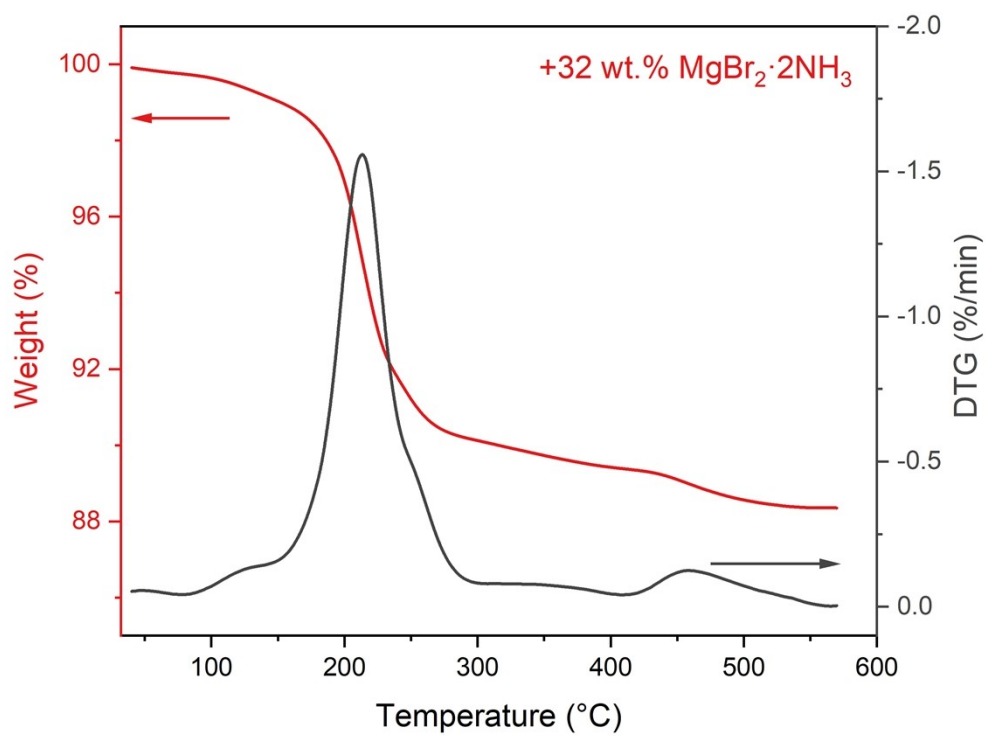
**Figure S6.** The TGA and DTG curves of $Mg(BH_4)_2 \cdot 1.9NH_3$-32 wt.% $MgBr_2 \cdot 2NH_3$ composite.

Figure S7. The XPS spectra of Mg(BH$_4$)$_2$·1.9NH$_3$-32 wt.% MgBr$_2$·2NH$_3$. Peak fitting reveals that

B 1s can be resolved into two peaks, assigned to B-H and B-O bonds, indicating the composite

surface contains oxygen. No new bonds were formed between MgBr$_2$·2NH$_3$ and Mg(BH$_4$)$_2$·1.9NH$_3$.
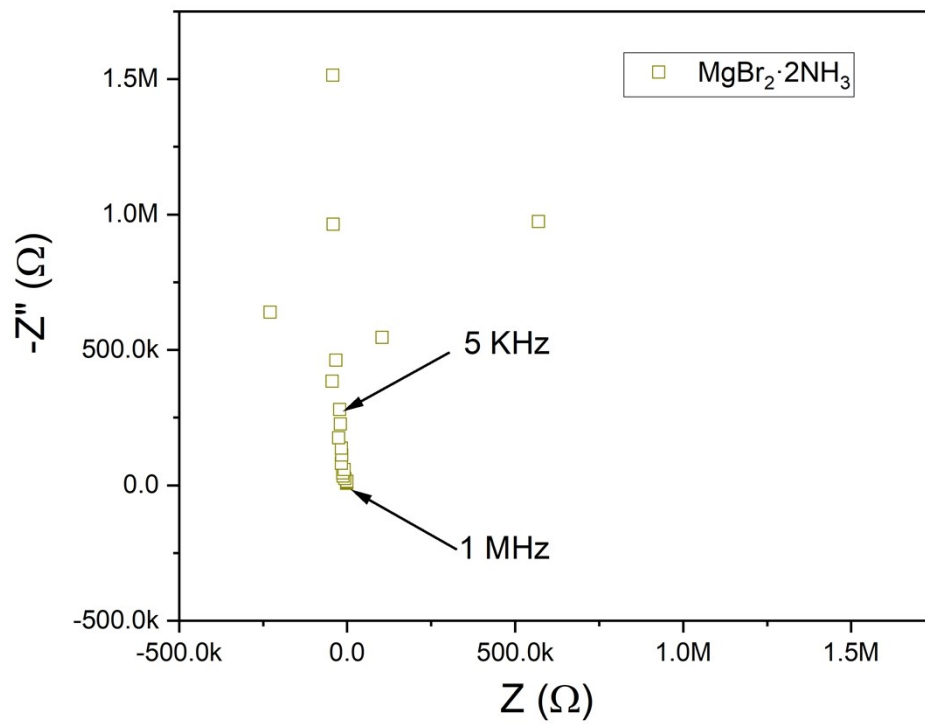
Figure S8. Nyquist plots of MgBr$_2$·2NH$_3$. MgBr$_2$·2NH$_3$ is not an Mg-ion conductor, as evidenced

by EIS measurement.
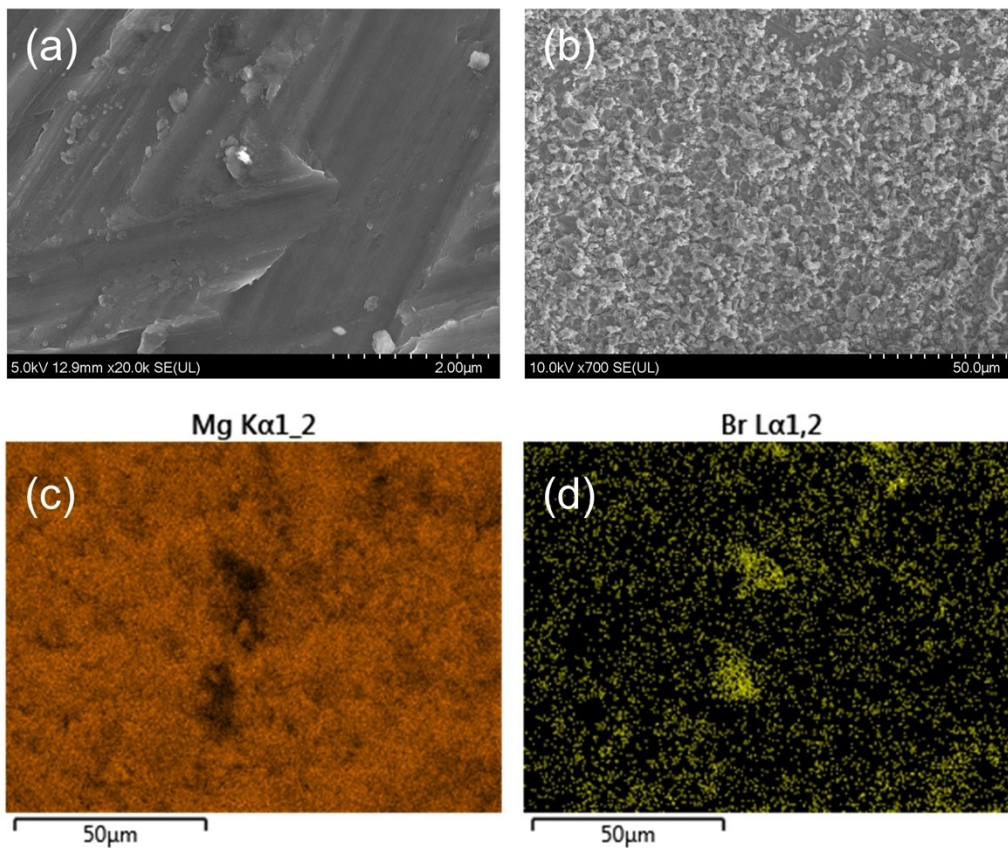
Figure S9. SEM images of Mg electrode. Compared to the pristine Mg electrode that has a flat surface, the surface of the Mg electrode after deposition is covered with flocculent. The elemental mapping in Figure S9 indicates the uniform Mg deposition, confirming the effective Mg migration through electrolyte to electrode. The observed Br signal on the surface of Mg electrode is owing to electrolyte residue.

Refences

1.   P. Zanella, L. Crociani, N. Masciocchi and G. Giunchi, *Inorg Chem*, 2007, **46**, 9039-9041.